

Point2Insert: Video Object Insertion via Sparse Point Guidance

Yu Zhou^{1,2,*}, Xiaoyan Yang^{1,*}, Bojia Zi^{1,3}, Lihan Zhang^{1,4}, Ruijie Sun^{1,5}, Weishi Zheng^{2,†}, Haibin Huang¹, Chi Zhang¹, Xuelong Li^{1,†}

¹Institute of Artificial Intelligence, China Telecom (TeleAI), ²Sun Yat-sen University, ³The Chinese University of Hong Kong, ⁴Tsinghua University, ⁵Fudan University

*Equal Contribution, [†]Corresponding Author

This paper introduces *Point2Insert*, a sparse-point-based framework for flexible and user-friendly object insertion in videos, motivated by the growing popularity of accurate, low-effort object placement. Existing approaches face two major challenges: mask-based insertion methods require labor-intensive mask annotations, while instruction-based methods struggle to place objects at precise locations. *Point2Insert* addresses these issues by requiring only a small number of sparse points instead of dense masks, eliminating the need for tedious mask drawing. Specifically, it supports both positive and negative points to indicate regions that are suitable or unsuitable for insertion, enabling fine-grained spatial control over object locations. The training of *Point2Insert* consists of two stages. In Stage 1, we train an insertion model that generates objects in given regions conditioned on either sparse-point prompts or a binary mask. In Stage 2, we further train the model on paired videos synthesized by an object removal model, adapting it to video insertion. Moreover, motivated by the higher insertion success rate of mask-guided editing, we leverage a mask-guided insertion model as a teacher to distill reliable insertion behavior into the point-guided model. Extensive experiments demonstrate that *Point2Insert* consistently outperforms strong baselines and even surpasses models with $\times 10$ more parameters.



1 Introduction

Video object insertion aims to integrate novel assets into dynamic scenes, serving as a keystone for modern visual effects, commercial content creation, and world model simulation Xing et al. (2024); Melnik et al. (2024); Croitoru et al. (2023); Ali et al. (2025); Polyak et al. (2024). Despite the rapid progress of generative video models Kling Team (2024); Team et al. (2025a); Gen-3 (2024); OpenAI (2024); Kong et al. (2024); Wiedemer et al. (2025), enabling *flexible* and *user-friendly* insertion with less manual effort remains a challenge.

Current editing methods primarily rely on two types of guidance: text instructions or dense masks. Instruction-based methods offer simplicity but often struggle with accurate object placement Bai et al. (2025); Team (2025a); Wu et al. (2025b); Deng et al. (2025); Labs et al. (2025); Wang et al. (2025); Team et al. (2025c); Huang et al. (2025). Conversely, mask-based methods are effective for spatial localization Bian et al. (2025); Jiang et al. (2025a); Li et al. (2022), but the quality of the masks significantly influences the insertion results. Manual mask annotation is time-consuming, especially for long or dynamic sequences. Although segmentation models Kirillov et al. (2023); Ravi et al. (2024); Carion et al. (2025); Chen et al. (2017) can automatically mask objects, they are limited to existing scene entities. When users wish to insert a novel object into an empty region, these models fail to provide position references. This motivates a critical question: *Can precise video insertion be achieved through sparse and easy interactions?*

Hence, we leverage points as a flexible and efficient input modality. **Point2Insert** is a video object insertion framework specifically designed to handle such sparse point inputs. It reformulates the insertion task as a point-guided process, thereby avoiding the need for labor-intensive mask annotations. A key feature of our



Figure 1 We present **Point2Insert**, a novel sparse point-guided framework designed for precise video object insertion. By leveraging a small number of sparse **positive** and **negative** points, our approach bypasses the need for tedious, frame-by-frame masking operations. *Point2Insert* handles diverse assets, capable of adding objects from people and animals to household items and background elements. Whether dealing with static or moving targets, or videos with moving cameras, *Point2Insert* consistently produces accurate results with low-effort control points.

approach is its support for both **positive and negative points**: positive points define the target placement, whereas negative points specify regions to be excluded. This positive–negative point interaction provides users with fine-grained position control over object insertion.

However, translating such sparse cues into dense video content presents an ill-posed mapping problem. To bridge the gap between sparse inputs and dense outputs, we develop a two-stage training strategy. In *Stage 1*, we train a foundational insertion model to add objects based on easily constructed datasets. In *Stage 2*, we fine-tune the model on paired videos generated via an advanced object removal model. This dense-to-sparse two stage training paradigm provides a smoother optimization path when adapting the model to sparse control. Furthermore, we introduce a mask-to-point distillation that transfers reliable insertion behaviors from a mask-guided teacher model to the point-guided model, helping to narrow the gap across different control signals.

We present a data construction pipeline for object-insertion video pairs and curate a large-scale dataset of 1.3M samples from real-world videos. Furthermore, we design **PointBench**, a benchmark featuring multi-dimensional evaluation metrics for insertion performance. Experiments show our method outperforms strong baselines in accurate insertion, including models ten times its size. Our method is capable of adding a wide variety of common objects, including food, people, and scenery, demonstrating broad applicability and practicality.

In summary, our contributions are as follows:

- **First point-guided video insertion framework.** We introduce a sparse interaction paradigm using positive and negative points, significantly reducing annotation overhead while maintaining precise position control.
- **Two-stage training with teacher distillation.** We propose a two-stage training pipeline that shifts from dense mask-based to sparse point-based control signals, with additional supervision provided by a mask-guided teacher model.
- **Comprehensive dataset and benchmark.** We construct a point-insertion dataset curated through object removal, along with a *PointBench* to evaluate point-based controllability, background preservation, temporal consistency, and visual fidelity.

2 Related Work

Recently, numerous video editing methods have been proposed, which can be categorized into two types: training-free and training-based approaches. Training-free methods typically employ DDIM inversion to transform latent into noise and then generate edited videos Geyer et al. (2024); Liu et al. (2024); Ku et al. (2024); Wu et al. (2023). These methods eliminate the need for extensive training and large-scale computational resources, but they often suffer from unstable editing results. In contrast, training-based methods require long training times on multiple GPUs Zhang et al. (2023); Zi et al. (2025c); Yang et al. (2025a); Mou et al. (2024); Jiang et al. (2025a); Bian et al. (2025); Wu et al. (2025a); Ye et al. (2025); Wei et al. (2025); Chen et al. (2025a), yet they produce more reliable and pleasing editing outcomes with lower inference costs. As a result, training-based approaches have become the mainstream in current video editing research Ma et al. (2025); Bao et al. (2024); Liu et al. (2025). Within this category, a subset of methods leverages masks to guide the editing location, enabling precise modifications while preserving the surrounding content. Other methods rely solely on textual instructions to insert objects into videos, with the editing model itself determining the placement.

Instruction-based methods. Instruction-based video editing has gained increasing popularity in recent years, leading to the emergence of numerous methods. Most existing studies focus on data curation. For instance, InsV2V Cheng et al. (2024) employs VideoP2P Liu et al. (2024) to curate training pairs and train editing models. Senorita-2M Zi et al. (2025b) constructs editing pairs using expert-designed editing strategies. Similarly, InsViE Wu et al. (2025a) leverages Stable Video Diffusion AI (2023) to propagate the edited image with the source video, which are subsequently filtered by GPT-4o Achiam et al. (2023) and other criteria to retain successful training pairs. Ditto Bai et al. (2025) provides fewer video pairs but offers higher resolution and longer video durations. OpenVE-3M He et al. (2025) mainly utilizes VACE Jiang et al. (2025a) and Wan2.1-Fun PAI (2023) to generate large-scale editing pairs, while ReCo Zhang et al. (2025) also releases a video editing dataset containing 500K editing pairs.

In contrast, other methods focus more on architecture design. UNIC Ye et al. (2025) proposes a model supporting in-context video editing. InstructX Mou et al. (2025) employs multimodal large language models (MLLMs) to guide the editing process. UniVideo Wei et al. (2025) and VINO Chen et al. (2026) unify video generation and editing, enabling object insertion using reference images. VideoCoF Yang et al. (2025c) modifies the model to incorporate chain-of-thought reasoning for improved editing performance. ICVE Liao et al. (2025) trains models on unpaired videos and subsequently performs supervised fine-tuning using filtered data. O-Disco-Edit Chen et al. (2025b) introduces object distortion control to flexibly support diverse editing cues within a unified representation. Beyond these general-purpose editors, several methods are specifically designed for object insertion. LoVoRA Xiao et al. (2025) jointly addresses object removal and insertion through learnable object-aware localization. Omni-Insert Chen et al. (2025a) builds a data curation pipeline to enable object insertion from arbitrary reference images. However, due to the difficulty of precisely describing an object’s location within a prompt, instruction-based editing methods still struggle to achieve accurate spatial placement in videos.

Mask-based methods. Video object insertion can be guided by masks. The most straightforward approach is to apply video inpainting methods with given textual prompts. AVID Zhang et al. (2023) is the first text-guided video inpainter based on diffusion models, which leverages an any-length technique to enable long video editing. COCOCO Zi et al. (2025c) introduces global damped attention and enhances textual cross-attention to achieve improved consistency and controllability. VideoPainter Bian et al. (2025) supports any-length video inpainting through a plug-and-play context control block, producing visually pleasing results by leveraging the first edited frame. VideoPivot Xie et al. (2025) performs multi-frame consistent image inpainting to generate coherent visual content within masked regions. VACE Jiang et al. (2025a) is a unified video editing framework capable of inpainting objects in specified masked areas. ReVideo Mou et al. (2024) utilizes motion information together with spatial masks to guide object inpainting in target regions. Unlike these inpainting methods, VideoAnyDoor Tu et al. (2025) is a training-free video object insertion method that achieves high-fidelity detail preservation and precise motion control. However, when performing object insertion tasks, it is challenging for users to provide accurate frame-by-frame masks. *Point2Insert* allows

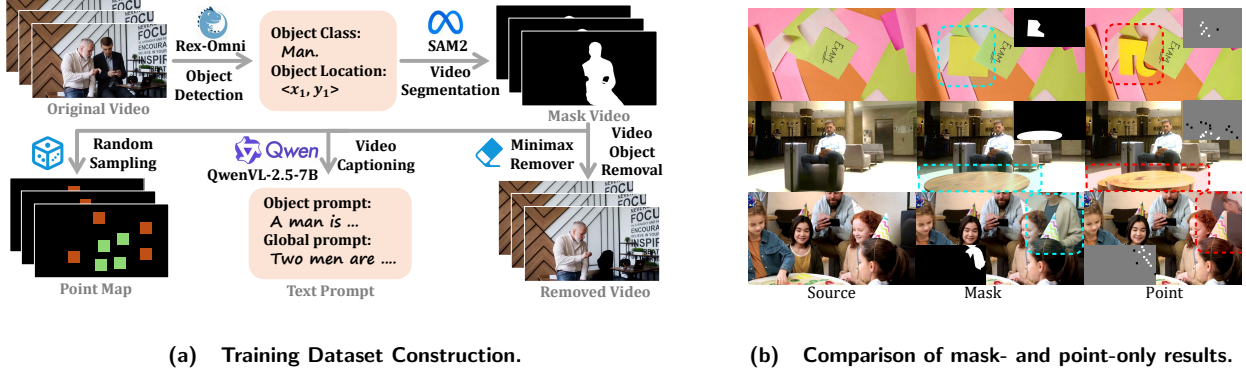


Figure 2 (a) Training Dataset Construction: Our pipeline detects objects within videos, extracts segmentation masks, removes the objects, and extracts video captions. Finally, we sample positive and negative points for training. **(b) Comparison of mask- and point-only results:** The mask-based setting generates more natural-looking objects due to explicit boundary cues. Point maps without clear boundaries often result in irregular shapes, geometric distortions, and blurred appearances.

users to specify the areas where objects should be added by clicking on the target regions, offering a more user-friendly sparse control signal.

3 Methodology

Overview. We summarize our approach in two training stages. In Stage 1, we train a model that accepts both masks and point inputs as guidance for object insertion in videos, using an easily constructed dataset. Unlike diffusion-based methods, our Stage-1 dataset does not rely on generative models; instead, we employ OpenCV with simple yet efficient traditional algorithms to build the dataset [Telea \(2004\)](#). The aim of stage-1 training is to build a model that can be used as the stage-2’s foundation, and serve as the stage-2’s teacher. In Stage 2, we utilize the minimax-remover [Zi et al. \(2025a\)](#) to curate a fine-grained video editing dataset. We then fine-tune the Stage-1 model with point-based guidance, while leveraging the mask-guided Stage-1 model as a teacher to further enhance the performance of the point-guided model.

3.1 Training Dataset Construction

We curate 1.3M video editing pairs from legally sourced Internet videos using recognition, segmentation, captioning, and object removal. Additionally, in stage-1 training, we used mask-inpainting synthetic data as a proxy for real removals.

3.1.1 Video Object Segmentation and Captioning

We detect objects in the first frame using Rex-Omni [Jiang et al. \(2025b\)](#) and segment them with SAM2 [Ravi et al. \(2025\)](#) to obtain video masks. Objects of extreme scales (i.e., occupying more than 50% or less than 0.5% of the frame area) are discarded. To balance object categories, we constrain the fraction of videos from the top 1% classes to at most 1%. Furthermore, we employ Qwen-VL2.5-7B [Team \(2025b\)](#) to caption the videos, generating both (1) global captions that describe scene context and spatial relations, and (2) object-level captions that capture appearance and pose. During training, we sample object captions, global captions, and class names in a 90:5:5 ratio to improve robustness.

3.1.2 Stage-1 Training Dataset Construction

The Stage-1 dataset is straightforward to construct. In this stage, the model receives two types of positional guidance (i.e., masks and points), corresponding to the masked video and the inpainted video, denoted as $\mathbf{x}_m, \mathbf{x}_{inp} \in \mathbb{R}^{f \times h \times w \times c}$, where $\mathbf{x}_m = \mathbf{x} \odot (\mathbf{1} - \mathbf{m})$, \mathbf{m} is the binary mask and \mathbf{x} is the original video. Importantly,

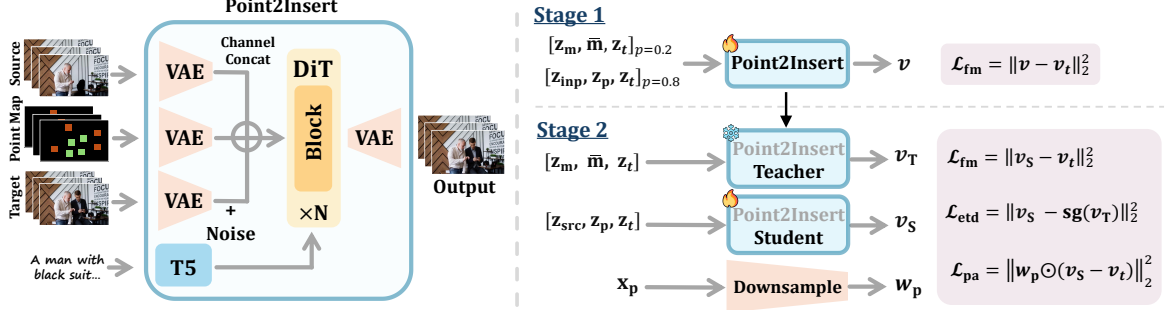


Figure 3 Model overview. The left panel illustrates that *Point2Insert* maps the source, point map, and target videos into a latent space via a VAE. These latents are concatenated channel-wise and processed by a DiT-based denoiser. The right panel details our two-stage training strategy: *Stage 1: Insertion Model Pre-training*. We use traditional lightweight inpainting to create source videos with objects removed. The DiT is then trained using a flow matching objective with maps generated via hybrid mask and point sampling. *Stage 2: Stronger Model Distillation*. A frozen teacher model from Stage 1 supervises a student model. While the teacher uses masks, the student employs point maps and source videos from a removal model. For further refinement, weight maps downsampled from the point-based map are applied to a weighted flow matching loss.

the inpainted video is not generated by diffusion models; instead, it is produced using a traditional inpainting algorithm [Telea \(2004\)](#). To unify the two types of position guidance, we convert the points into the point map, denoted as $\mathbf{x}_p \in \mathbb{R}^{f \times h \times w \times c}$, having the same dimension as the mask \mathbf{m} . In particular, we extend several pixels from the point center to the surrounding area, thereby constructing a square region. Within this region, positive points are assigned a value of 1, negative points are assigned a value of 0.5, and the background is set to 0. As the construction process is computationally efficient, these videos are generated online during training.

3.1.3 Stage-2 Training Dataset Construction

The automated pipeline is shown in Fig. 2 a. We leverage SOTA object remover to synthesize training pairs $(\mathbf{x}_{src}, \mathbf{x})$ by removing objects from original videos $\mathbf{x} \in \mathbb{R}^{f \times h \times w \times c}$, effectively treating insertion as the inverse of removal. The point map curation is same as the stage-1.

3.2 Stage-1 Training: Pretrain An Insertion Model

The objective of stage-1 training is to build a foundation model for stage-2 and to serve as a teacher that improves the performance of the point-guided video editor in stage-2. To achieve this, we use masked videos \mathbf{x}_m together with masks \mathbf{m} to train the mask-guided video insertion model, and employ inpainting videos \mathbf{x}_{inp} along with point maps \mathbf{x}_p to train the foundation model. Since both types of inputs share the same dimensionality, we unify them into a single model with a unified training process. During inference, the model determines the editing task based on whether the input video contains corrupted regions, eliminating the need for additional control signals to distinguish between the two editing tasks.

During training, we employ the autoencoder \mathcal{E} to encode the video conditions into latent representations. Specifically, the masked video \mathbf{x}_m is encoded as \mathbf{z}_m , and the corresponding mask is encoded as $\bar{\mathbf{m}}$. The original video \mathbf{x} is encoded into \mathbf{z} . Similarly, the inpainted video \mathbf{x}_{inp} and the point map \mathbf{x}_p are encoded into \mathbf{z}_{inp} and \mathbf{z}_p , respectively. Given a timestep $t \in [0, 1]$, the noisy latent is constructed as $\mathbf{z}_t = t \cdot \epsilon + (1 - t) \cdot \mathbf{z}$, where $\epsilon \sim \mathcal{N}(0, I)$, following the flow matching training strategy proposed in [Lipman et al. \(2022, 2024\)](#).

For the mask-guided task, we concatenate \mathbf{z}_m , $\bar{\mathbf{m}}$, and \mathbf{z}_t along the channel dimension and feed the resulting representation into the DiT model with a probability of $p = 0.2$, while for the point-guided task, we concatenate \mathbf{z}_{inp} , \mathbf{z}_p , and \mathbf{z}_t in the same manner and input them into the DiT model with a probability of $p = 0.8$. To accommodate these heterogeneous inputs, we replace the original patch embedder of the DiT model with a new patch embedder that supports 48 input channels.

3.3 Stage-2 Training: Distill An Stronger Insertion Model

While point-based interaction offers great convenience for users, training a robust model under such sparse conditions face a challenge. There is a significant performance gap exists between discrete points and the dense masks used in object insertion, as shown in Fig. 2 b. Intuitively, denser information helps the model produces more consistent motion and precise location. Therefore, only using sparse signal to guide the insertion model’s training often leads to slow convergence and suboptimal performance. To bridge this gap, we propose a distillation strategy [Hinton et al. \(2015\)](#) by finetuning the stage-1 model with points guidance supervised by mask-guided teacher.

Explicit Teacher Distillation. Here, we introduce explicit teacher distillation to achieve goal of the generation consistency between point-based and mask-based model. The following is our distillation loss:

$$\begin{aligned}\mathcal{L}_{\text{etd}} &= \|\mathbf{v}_S - \text{sg}(\mathbf{v}_T)\|_2^2, \\ \mathbf{v}_S &= u_{\text{student}}(\mathbf{z}_{\text{src}}, \mathbf{z}_p, \mathbf{z}_t, \mathbf{c}_{\text{txt}}, t; \theta_S), \\ \mathbf{v}_T &= u_{\text{teacher}}(\mathbf{z}_m, \bar{\mathbf{m}}, \mathbf{z}_t, \mathbf{c}_{\text{txt}}, t; \theta_T).\end{aligned}\quad (1)$$

where, $\text{sg}(\cdot)$ is the stop gradient operation, the θ_S and θ_T are the parameters of the student u_{student} and teacher model u_{teacher} , respectively. \mathbf{c}_{txt} is the text condition encoded by T5 [Raffel et al. \(2020\)](#). The \mathbf{v}_S and \mathbf{v}_T are the output of the student and teacher model, while \mathbf{v}_t is the velocity: $\mathbf{v}_t = \epsilon - \mathbf{z}$.

By enforcing output consistency across different guidance types, distillation bridges the performance gap between dense masks and sparse points.

Point-Aware Enhancement. Since control points occupy only a negligible fraction of the pixel space, we introduce a point-aware enhancement loss to address signal sparsity. We transform the point map \mathbf{x}_p into weight map \mathbf{w}_p to reweight the distillation loss, aiming to force model focus on the small but critical regions.

To ensure the point map $\mathbf{x}_p \in \mathbb{R}^{f \times h \times w \times c}$ matches the dimensions of the target latent $\mathbf{z}_t \in \mathbb{R}^{(\frac{f-1}{4}+1) \times \frac{h}{8} \times \frac{w}{8} \times c'}$, where $c' = 16$ in current mainstream video diffusion models. we employ a spatial-temporal average pooling operator \mathcal{T} . The strides are $1 \times 8 \times 8$ for the first frame and $4 \times 8 \times 8$ for subsequent frames. We then repeat the first channel with c' times to align the weight channels with the latent space. Unlike direct downsampling by the VAE encoder, the pooling operation maps the source point map to the weight map in a continuous manner, assigning higher weights to regions with higher point density.

Consequently, given the ground-truth velocity $\mathbf{v}_t = \epsilon - \mathbf{z}$, the loss \mathcal{L}_{pa} is defined as:

$$\begin{aligned}\mathcal{L}_{\text{pa}} &= \|\mathbf{w}_p \odot (\mathbf{v}_S - \mathbf{v}_t)\|_2^2, \\ \mathbf{w}_p &= |\mathcal{T}(\mathbf{x}_p) - 0.5|.\end{aligned}\quad (2)$$

This weighting strategy encourages model to focus on annotated locations, ensuring modification on editable regions and preservation on uneditable regions, respectively.

Background Alignment. However, the current video object remover is not fully reliable, as it occasionally generates unacceptable results. These flawed cases within the training dataset can adversely affect the learning process. The majority of failures stem from background inconsistencies, which cause the editing model to produce incoherent backgrounds and thereby degrade the overall generation quality. To address this issue, we apply dilation and feathering to the point map, followed by compositing the input video’s background onto the target frames. This approach ensures consistent background reconstruction while effectively eliminating potential boundary artifacts.

Training Objective. The final training loss \mathcal{L} is defined as a weighted combination of the control and generative terms:

$$\mathcal{L} = \mathcal{L}_{\text{fm}} + \lambda_1 \mathcal{L}_{\text{etd}} + \lambda_2 \mathcal{L}_{\text{pa}}, \quad (3)$$

where coefficients λ_1 and λ_2 weight the trade-off between distillation guidance and sparse point control. The flow-matching loss \mathcal{L}_{fm} is defined as the discrepancy between the student output \mathbf{v}_S and the ground-truth target \mathbf{v}_t .

4 Experiments

4.1 Implementation Details

Training Details. Our method is built upon the WAN2.1-T2V-1.3B [Wan et al. \(2025\)](#). To accommodate varying resolutions, we employ a dynamic resolution strategy using buckets ranging from $240 \times 240 \times 1$ to $832 \times 832 \times 121$, with an interval of $16 \times 16 \times 4$. The training process consists of two stages, both optimized using AdamW [Loshchilov and Hutter \(2019\)](#) ($\beta_1 = 0.9, \beta_2 = 0.99$). **Stage I.** We train the model for 5,000 steps on a mixture of masked (80%) and inpainted (20%) video data. This stage uses a batch size of 128 and a learning rate of 5×10^{-5} . **Stage II.** We further fine-tune the model for 5,000 steps on object removal tasks with a reduced learning rate of 1×10^{-5} . We set loss weights $\lambda_1 = 1.5$ and $\lambda_2 = 1.2$. To enhance insertion across different point density, we sample insertion prompts according to the following distribution: masks (10%), sparse points (30%), and dense points (60%).

Benchmark. To evaluate our point-based insertion model, we establish *PointBench*, which consists of two specialized subsets:

- *Point-based Control:* We utilize the DAVIS testset [Perazzi et al. \(2016\)](#), which contains 90 videos characterized by rapid motion, significant blur, and complex occlusions. For each video, we sample keyframes at 10-frame intervals and manually annotate positive and negative points, alongside descriptive text for the target objects.
- *Mask-based Control:* We collect 100 diverse web videos covering both indoor and outdoor scenery. Leveraging Qwen-VL [Team \(2025b\)](#) and SAM2 [Ravi et al. \(2025\)](#), we implement an automated pipeline to extract object-level prompts and masks to construct evaluation pairs.

Metrics. We evaluate 11 metrics across four dimensions:

- *Point Response Accuracy.* We employ Sa2va [Perazzi et al. \(2016\)](#) to segment the newly added objects and calculate the hit rate for positive and negative points within the predicted masks.
- *Background Preservation.* We compute PSNR [Wikipedia contributors \(2024\)](#), LPIPS [Zhang et al. \(2018\)](#), SSIM [Wang et al. \(2004\)](#), MSE, and MAE specifically within the unmasked regions to assess reconstruction quality.
- *Text Alignment.* We evaluate text-video alignment (CLIP-TA) by comparing the generated frames with the object insertion prompts. Additionally, background semantic preservation (CLIP-BG) is measured by comparing the background regions against the global scene captions.
- *Temporal Consistency.* We utilize Ewarp (pixel-level) and CLIP-TC (semantic-level) to quantify the discrepancy between consecutive frames, with results averaged across the entire video sequence.

Baselines. We evaluate *Point2Insert* against several state-of-the-art video editing methods, categorized into two groups: (i) **mask-based** methods, including VideoPainter [Bian et al. \(2025\)](#), Vace [Jiang et al. \(2025a\)](#), and Senorita [Zi et al. \(2025b\)](#); and (ii) **instruction-based** approaches, such as Ditto [Bai et al. \(2025\)](#), Lucy [Team \(2025a\)](#), VideoCof [Yang et al. \(2025c\)](#), ICVE [Liao et al. \(2025\)](#), and UniVideo [Wei et al. \(2025\)](#). Although Senorita is a mask-free video propagation model, it requires a mask to edit the first frame. Since some baselines do not natively support point-based or mask-based control, we adapt their inputs to ensure a fair comparison:

- *Instruction-based models:* To convert point or mask inputs into textual prompts, we employ Qwen2.5-VL-7B [Team \(2025b\)](#) to translate these annotations into text descriptions that specify the target locations.
- *Mask-based models:* To convert point inputs into masks, we compute the convex hull of the input points on each keyframe and apply the resulting masks consistently across the entire video.

Table 1 Quantitative comparison of Point2Insert and video editing models on PointBench. Evaluation consists of two parts: (1) using point maps as input on the DAVIS dataset, and (2) using mask as input on an internal test dataset. We compare against both instruction-based models: Ditto [Bai et al. \(2025\)](#), Lucy [Team \(2025a\)](#), ICVE [Liao et al. \(2025\)](#), Senorita [Zi et al. \(2025b\)](#), UniVideo [Wei et al. \(2025\)](#) and VideoCoF [Wei et al. \(2025\)](#), and mask-based models: VideoPainter [Bian et al. \(2025\)](#) and VACE [Jiang et al. \(2025a\)](#). Evaluation metrics include success rate in responding to the provided control conditions, Background preservation in unedited regions, Text-alignment quality, and Inter-frame consistency. **Red** indicates the best, and **blue** denotes the second. Our model has only **1.3B** parameters, yet it outperforms other models that are **10 \times** larger in scale. Model parameter details are provided in Appendix [section D](#).

Point-Based Eval		Acc _{pos} \uparrow	Acc _{neg} \uparrow	MSE \downarrow	MAE \downarrow	PSNR \uparrow	SSIM \uparrow	LPIPS _{$\times 100$} \downarrow	CLIP BG \uparrow	CLIP TA \uparrow	CLIP TC \uparrow	Ewarp _{$\times 100$} \downarrow
Instruction.	Ditto	22.07	81.99	5179.42	53.47	12.28	0.4298	36.33	21.95	22.01	97.41	7.19
	Lucy	16.19	89.29	449.69	11.70	23.09	0.7441	13.32	24.20	22.92	96.21	6.97
	ICVE	14.65	90.39	848.60	15.39	23.23	0.7328	12.69	24.48	22.99	95.91	9.32
	UniVideo	15.73	84.87	2419.20	29.22	16.29	0.5054	24.34	24.08	23.39	96.82	6.45
	VideoCoF	8.15	93.51	341.80	12.20	23.95	0.8184	7.22	24.05	22.42	96.27	5.77
Mask.	Senorita	49.63	94.73	225.28	6.98	26.94	0.8201	7.29	24.85	23.66	96.76	6.02
	VideoPainter	68.36	88.70	226.38	9.02	25.50	0.8142	8.00	24.99	23.36	96.49	6.31
	Vace	16.04	94.87	140.88	6.40	28.22	0.8444	5.21	24.74	22.74	96.82	6.28
Ours		81.13	96.87	93.19	5.39	29.51	0.8592	4.49	25.55	23.68	96.86	6.25
Mask-Based Eval		Model Size	MSE \downarrow	MAE \downarrow	PSNR \uparrow	SSIM \uparrow	LPIPS _{$\times 100$} \downarrow	CLIP BG \uparrow	CLIP TA \uparrow	CLIP TC \uparrow	Ewarp _{$\times 100$} \downarrow	
Instruction.	Ditto	14B	7877.31	70.03	12.07	0.6286	37.60	16.82	17.53	99.32	0.41	
	Lucy	5B	662.92	9.18	27.85	0.9017	7.66	23.15	21.74	99.08	0.57	
	ICVE	13B	2998.15	35.64	20.10	0.7993	14.06	23.83	22.32	99.20	0.74	
	UniVideo	13B+7B	813.82	13.94	21.27	0.7320	10.92	23.76	22.66	99.18	0.37	
	VideoCoF	14B	442.63	9.73	25.58	0.9171	7.23	23.38	22.06	99.15	0.29	
Mask.	Senorita	5B+12B	106.35	4.78	30.91	0.9445	4.25	24.66	22.91	99.31	0.34	
	VideoPainter	5B+12B	205.24	4.31	29.24	0.9520	3.84	24.52	23.14	99.26	0.39	
	Vace	1.3B+0.3B	164.84	3.74	32.18	0.9566	3.25	24.32	22.73	99.11	0.49	
Ours		1.3B	103.09	2.59	35.72	0.9694	2.02	24.53	23.11	99.27	0.32	

4.2 Experimental Results

Quantitative Comparisons. Tab. 1 presents the quantitative comparisons on *PointBench*. *Point2Insert* demonstrates strong performance under sparse point control. The upper part of Tab. 1 presents the quantitative comparison in point setting. Specifically, our method performs best in control accuracy, outperforms the second-best method by 12.77% and 8.17% in Acc_{pos} and Acc_{neg}, indicating our ability to accurately respond to the point control and insert objects that satisfy both positive and negative constraints.

In terms of background preservation, *Point2Insert* ranks first in all five metrics, capability to avoid background interference while performing local additions. In contrast, methods such as UniVideo and Ditto suffer from noticeable performance degradation due to interference with the overall video style. Additionally, *Point2Insert* maintains competitive performance in text alignment and temporal consistency, including CLIP-BG, CLIP-TA, and CLIP-TC. Overall, these results show that *Point2Insert* effectively adds objects under sparse control, successfully balancing control accuracy, generation quality, background preservation, and temporal consistency.

In the mask-based editing task, *Point2Insert* also outperforms most baselines. It leads the second-best VACE by 3.54 in PSNR, by 1.23 in LPIPS, and exhibits superior background preservation. In the only metric where we are not in the top two, CLIP-TC, we are just 0.05% behind the top performer. This demonstrates that our model performs equally well on mask-based editing tasks. The consistently strong performance across both point- and mask-based tasks highlights the effectiveness of our method in handling both sparse and dense control signals.

Qualitative Comparisons. Fig. 4 presents a qualitative comparison between our approach and state-of-the-art video editing methods. Because the initial frames of VideoPainter and Senorita are generated by external image editing models, which do not fully reflect the core video editing capabilities of these frameworks, we selected random middle frames for a more objective comparison. The top row displays the original input frames with a black overlay, where green and red **points** indicate editable and non-editable regions.



Figure 4 Qualitative comparison of video object insertion. Source videos (top) with a dark overlay contain sparse **editable** and **uneditable** points. To ensure a fair comparison, we adapt the input to handle these sparse signals: for *instruction-based* models, QwenVL Team (2025b) translates source videos with markers into textual position prompts; for *mask-based* models, the convex hull of the positive points across all keyframes is used as the input mask. In contrast, *Point2Insert* directly consumes sparse point maps. **Bounding boxes** highlight specific artifacts: **incorrect editing or wrong placement** and **insertion failure or unintended removal**. Our method outperforms other methods in both photorealism and localization accuracy.

Table 2 Quantitative Evaluation of Generation Quality. We evaluate the generation quality of methods on *PointBench* using a large multimodal language model (MLLM). The MLLM assesses object insertion success rate (**Succ.**), semantic alignment between the generated object and the textual description (**Sem.**), and the visual quality of the generated object (**Qual.**).

Method	GPT5.2			Gemini3Pro		
	Succ.(%)↑	Sem.↑	Qual.↑	Succ.(%)↑	Sem.↑	Qual.↑
Lucy	28.89	1.42	1.55	21.11	1.50	1.45
Ditto	35.56	1.80	2.03	25.56	1.69	1.45
ICVE	20.00	1.39	1.57	20.00	1.61	1.58
UniVideo	36.67	1.80	1.97	24.44	1.87	1.77
VideoCof	10.00	1.14	1.32	7.78	1.14	1.14
Senorita	56.18	1.68	2.04	56.18	2.23	1.90
Video Painter	82.02	2.01	2.31	76.40	2.64	2.14
Vace	18.89	1.34	1.59	20.00	1.42	1.50
Ours	91.11	2.52	2.83	94.44	3.69	3.57

Bounding boxes highlight specific artifacts: red boxes denote misplacement, while cyan boxes indicate insertion failures. Despite being provided with location instructions, current instruction-based methods lack sufficient positioning accuracy. Especially in scenarios with large regions of overall similar appearance (e.g., the rocks in column 1), these models fail to accurately localize the target location and have difficulty interpreting directional prompts such as *left* or *right*. Furthermore, the results of Ditto, ICVE, and Lucy are highly unstable, sometimes failing to insert the object. Additionally, VideoCoF even erroneously removes the swan’s head (column 2) and the black car’s front wheel (column 5).

Since mask-based methods require per-frame annotations, we use the convex hull mask of the point ranges as a proxy, which is inherently imprecise. In these cases, Senorita and VideoPainter tend to fill the entire mask, while VACE consistently fails to add any objects when handling such irregular, non-semantic masks. In contrast, our method outperforms existing approaches in both visual fidelity and localization accuracy, demonstrating robust object insertion even on DAVIS testset with significant camera motion.

4.3 MLLM Evaluation

Tab. 2 reports the quantitative evaluation of editing quality on *PointBench* using Gemini3-Pro [Team et al. \(2025b\)](#). Overall, our method achieves strong performance across metrics such as object insertion success, semantic alignment, and visual quality, outperforming most baselines. While Video Painter attains comparable results, it relies on a significantly larger model size (5B + 12B vs. our 1.3B) and requires additional first-frame image editing; in contrast, our method is more lightweight and versatile. Moreover, VLM-based models struggle to determine whether the inserted objects are placed at the correct locations with respect to the given control conditions. Consequently, our superiority in this aspect is more clearly reflected by the Acc_{pos} and Acc_{neg} scores in Tab. 1.

4.4 Ablation Analysis and Hyperparameter Tuning

We perform ablation studies and hyperparameter tuning to assess method components, point densities, and point sizes.

Effects of Explicit Teacher Distillation and Point-Aware Enhancement. We conduct ablation studies on the effects of the point-aware control loss \mathcal{L}_{pa} and the distillation loss \mathcal{L}_{etd} , as shown in Tab. 3. Introducing the point-aware loss \mathcal{L}_{pa} leads to a clear improvement in control accuracy, with the positive control accuracy Acc_{pos} increasing from 74.36% to 78.26%. These results indicate that \mathcal{L}_{pa} effectively enforces point-level constraints, thereby improving the model’s control over object location and structure.

By comparing settings with and without the explicit teacher distillation loss \mathcal{L}_{etd} , we observe additional gains in both control accuracy and generation quality when teacher guidance is introduced. Specifically,

Table 3 Ablation Studies on Point2Insert Method Components. We perform ablation studies on the DAVIS subset of *PointBench*. In this context, \mathcal{L}_{pa} denotes the point-aware control loss, and \mathcal{L}_{etd} represents the explicit teacher distillation loss.

	$\mathbf{Acc}_{\text{pos}} \uparrow$	$\mathbf{Acc}_{\text{neg}} \uparrow$	$\mathbf{MSE} \downarrow$	$\mathbf{PSNR} \uparrow$	$\mathbf{LPIPS}_{\times 100} \downarrow$	$\mathbf{CLIP \ BG} \uparrow$	$\mathbf{CLIP \ TA} \uparrow$
w/o \mathcal{L}_{pa}	74.36	98.04	97.87	29.15	4.60	25.80	23.73
w/ \mathcal{L}_{pa}	78.26	97.89	95.24	29.38	4.55	25.73	23.70
w/o \mathcal{L}_{etd}	78.93	96.35	101.08	29.10	4.63	25.68	23.73
w/ \mathcal{L}_{etd}	79.77	97.33	94.74	29.49	4.51	25.74	23.64

Table 4 Ablation Study on Different Point Density. In this context, **First frame** refers to applying control signals only to the first frame. **Fixed density** refers to applying control signals at specified keyframes with a fixed spatial sampling density. **Variable density** refers to applying control signals at specified keyframes with varying spatial sampling densities.

	$\mathbf{Acc}_{\text{pos}} \uparrow$	$\mathbf{Acc}_{\text{neg}} \uparrow$	$\mathbf{MSE} \downarrow$	$\mathbf{PSNR} \uparrow$	$\mathbf{LPIPS}_{\times 100} \downarrow$	$\mathbf{CLIP \ BG} \uparrow$	$\mathbf{CLIP \ TA} \uparrow$
First frame	65.14	97.39	93.60	29.46	4.57	25.60	23.64
Fixed ratio	72.94	97.51	95.82	29.29	4.57	25.52	23.52
Various ratio	74.36	98.04	97.87	29.15	4.60	25.80	23.73

$\mathbf{Acc}_{\text{pos}}/\mathbf{Acc}_{\text{neg}}$ improve by nearly 1%, and PSNR increases by 0.3, while semantic alignment remains stable. These results demonstrate that explicit teacher distillation provides complementary supervision, contributing to improved overall generation quality.

Effects of Point Density. In Tab. 4, we conduct an ablation study on different control settings, including sampling only at the first frame (First frame), sampling at keyframes with a fixed point density (Fixed density), and sampling at keyframes with varying point densities (Variable density).

Sampling points only from the first frame leads to a significant performance degradation, with $\mathbf{Acc}_{\text{pos}}$ dropping by 7.8%. This is because the control signals are too sparse, causing the model to fail to insert objects in subsequent frames, which leads to unstable object generation and temporal flickering. In contrast, sampling at keyframes helps mitigate this issue. Among three setting, the various sampling ratio achieve the best overall performance, with $\mathbf{Acc}_{\text{pos}}$ and $\mathbf{Acc}_{\text{neg}}$ increasing by 1.42% and 0.53%, respectively. These results demonstrate the model’s strong generalization capability across varying point densities.

Effects of Point Size. In Tab. 5, we study the impact of different point sizes, specifically 2, 6, 10, 20, and 30. The results show that both excessively small and excessively large point sizes lead to a noticeable drop in accuracy. In particular, using a very extreme point sizes of 2 and 30 results in a 15.72% and 16.52% drops in $\mathbf{Acc}_{\text{pos}}$, respectively. This is because small point sizes produce weak control, which are often ignored by the model and lead to object insertion failures in some cases, whereas large point sizes reduce control flexibility. In contrast, point sizes of 10 and 20 achieve the highest and second-highest $\mathbf{Acc}_{\text{pos}}$ scores, respectively. Overall, these results indicate that point sizes in the range of 10–20 provide a better trade-off between control strength and flexibility, which aligns with the scale of the model’s 16×16 patch downsampling factor.

5 Conclusion and Discussion

In this paper, we present *Point2Insert*, a point-based framework for user-friendly video object addition that introduces three key innovations: unified representation integrating point and mask control inputs; a mask-guided object insertion model distilled into a point-guided model, enabling performance comparable to mask-based methods even with sparse point inputs; and a large-scale dataset comprising 1.3M video pairs, along with a benchmark designed to evaluate the effectiveness of current object addition models. Extensive experiments demonstrate that *Point2Insert* achieves state-of-the-art results in both precise control and visual

Table 5 Ablation Study on Different Point Size. Results are more effective when the point size corresponds to the receptive field pixels of one visual token.

Grid Size	Acc _{pos} \uparrow	Acc _{neg} \uparrow	MSE \downarrow	PSNR \uparrow	LPIPS _{$\times 100$} \downarrow	CLIP BG \uparrow	CLIP TA \uparrow
2	57.51	94.40	98.11	29.26	4.63	25.63	23.68
6	70.28	96.28	99.89	29.40	4.61	25.60	23.58
10	72.78	95.32	108.82	29.10	4.69	25.68	23.73
20	70.98	96.63	105.23	29.23	4.71	25.69	23.71
30	56.26	96.43	92.81	29.49	4.59	25.59	23.61

quality. Nevertheless, *Point2Insert* also has limitations: when global prompts are applied, object insertion capability slightly degrades due to the imprecise description; and the editing quality is constrained by the base model’s relatively small size (1.3B parameters). We anticipate that scaling to larger models will enhance performance in complex scenes and further improve visual quality.

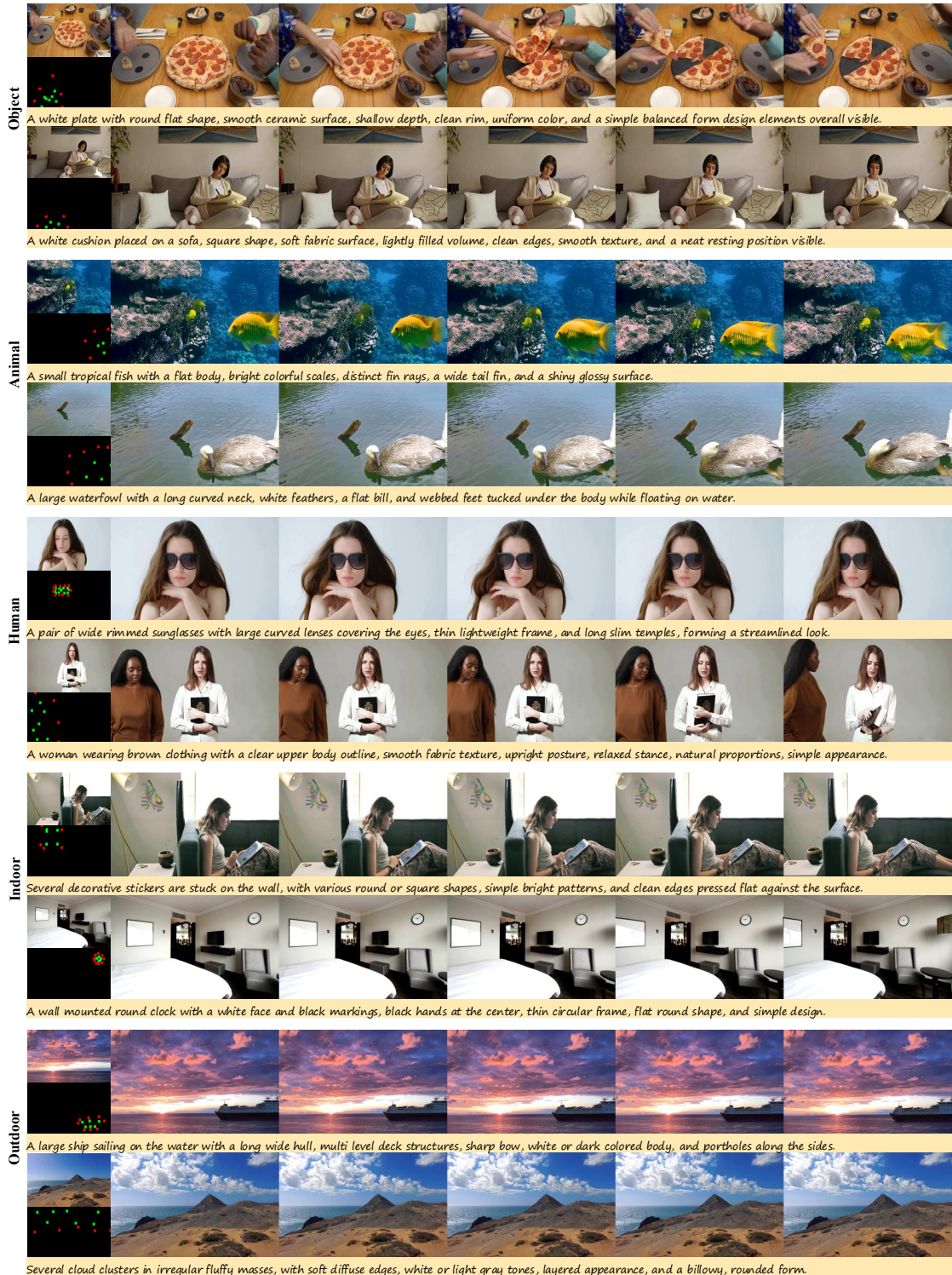


Figure 5 More video object insertion results.

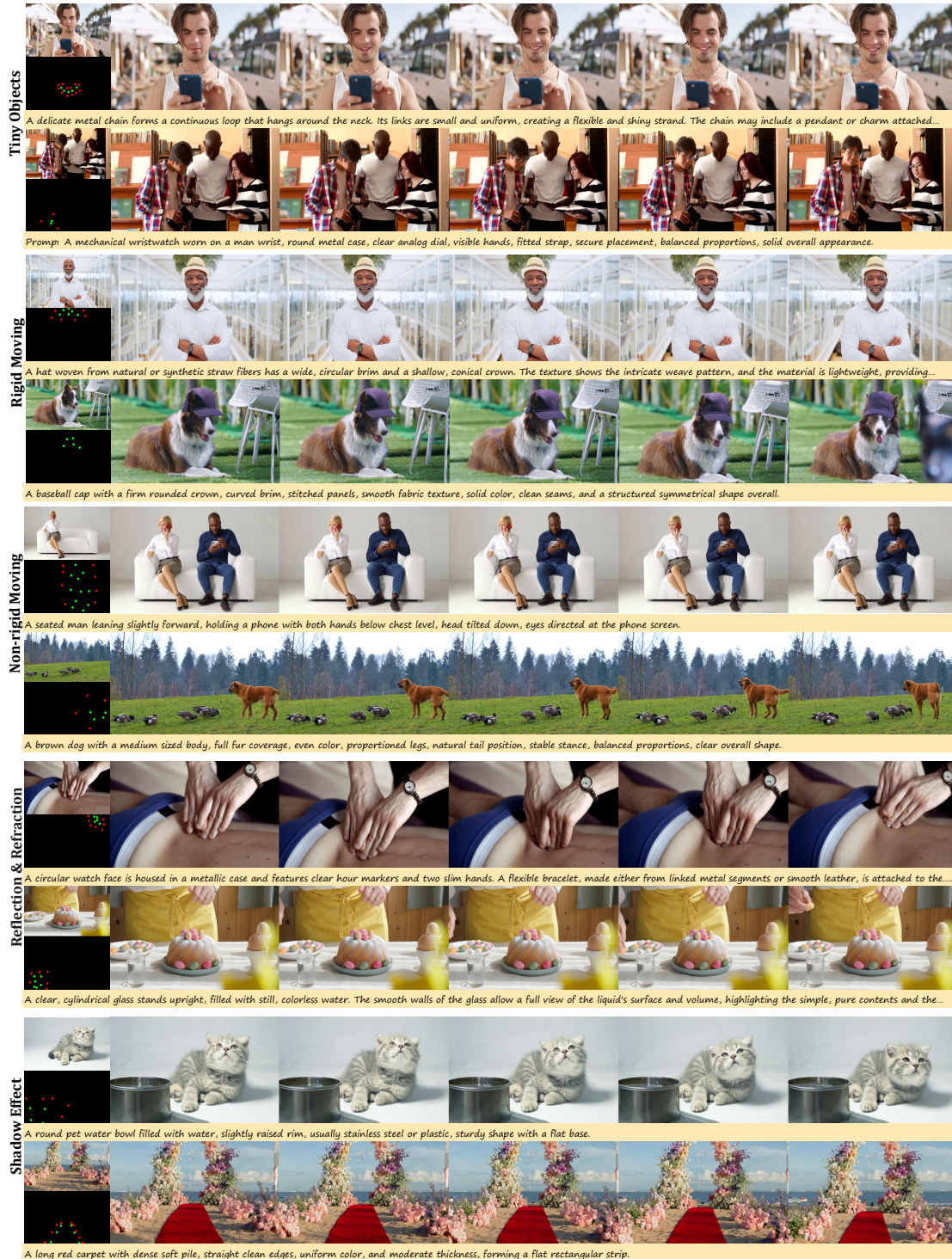


Figure 6 More video object insertion results.

References

- Josh Achiam, Steven Adler, Sandhini Agarwal, Lama Ahmad, Ilge Akkaya, Florencia Leoni Aleman, Diogo Almeida, Janko Altenschmidt, Sam Altman, Shyamal Anadkat, et al. 2023. Gpt-4 technical report. *arXiv preprint arXiv:2303.08774* (2023).
- Stability AI. 2023. Stable Video Diffusion. <https://stability.ai/stable-video>. Accessed: 2026-01-09.
- Arslan Ali, Junjie Bai, Maciej Bala, Yogesh Balaji, Aaron Blakeman, Tiffany Cai, Jiaxin Cao, Tianshi Cao, Elizabeth Cha, Yu-Wei Chao, et al. 2025. World simulation with video foundation models for physical ai. *arXiv preprint arXiv:2511.00062* (2025).
- Qingyan Bai, Qiuyu Wang, Hao Ouyang, Yue Yu, Hanlin Wang, Wen Wang, Ka Leong Cheng, Shuailei Ma, Yanhong Zeng, Zichen Liu, et al. 2025. Scaling Instruction-Based Video Editing with a High-Quality Synthetic Dataset. *arXiv preprint arXiv:2510.15742* (2025).
- Fan Bao, Chendong Xiang, Gang Yue, Guande He, Hongzhou Zhu, Kaiwen Zheng, Min Zhao, Shilong Liu, Yaole Wang, and Jun Zhu. 2024. Vidu: a highly consistent, dynamic and skilled text-to-video generator with diffusion models. *arXiv preprint arXiv:2405.04233* (2024).
- Yuxuan Bian, Zhaoyang Zhang, Xuan Ju, Mingdeng Cao, Liangbin Xie, Ying Shan, and Qiang Xu. 2025. VideoPainter: Any-length Video Inpainting and Editing with Plug-and-Play Context Control. In *SIGGRAPH*.
- Black Forest Labs. 2024. Black Forest Labs. <https://github.com/black-forest-labs/flux/>.
- Nicolas Carion, Laura Gustafson, Yuan-Ting Hu, Shoubhik Debnath, Ronghang Hu, Didac Suris, Chaitanya Ryali, Kalyan Vasudev Alwala, and et al. Haitham Khedr. 2025. SAM 3: Segment Anything with Concepts. *arXiv preprint arXiv:2511.16719* (2025).
- Junyi Chen, Tong He, Zhoujie Fu, Pengfei Wan, Kun Gai, and Weicai Ye. 2026. VINO: A Unified Visual Generator with Interleaved OmniModal Context. *arXiv preprint arXiv:2601.02358* (2026).
- Jinshu Chen, Xinghui Li, Xu Bai, Tianxiang Ma, Pengze Zhang, Zhuowei Chen, Gen Li, Lijie Liu, Songtao Zhao, Bingchuan Li, and Qian He. 2025a. OmniInsert: Mask-Free Video Insertion of Any Reference via Diffusion Transformer Models. *arXiv:arXiv:2509.17627*
- Liang-Chieh Chen, George Papandreou, Iasonas Kokkinos, Kevin Murphy, and Alan L Yuille. 2017. Deeplab: Semantic image segmentation with deep convolutional nets, atrous convolution, and fully connected crfs. *IEEE transactions on pattern analysis and machine intelligence* 40, 4 (2017), 834–848.
- Yuqing Chen, Junjie Wang, Lin Liu, Ruihang Chu, Xiaopeng Zhang, Qi Tian, and Yujiu Yang. 2025b. O-DisCo-Edit: Object Distortion Control for Unified Realistic Video Editing. *ArXiv:2509.01596* (2025).
- Jiaxin Cheng, Tianjun Xiao, and Tong He. 2024. Consistent Video-to-Video Transfer Using Synthetic Dataset. In *ICLR*.
- Florinel-Alin Croitoru, Vlad Hondu, Radu Tudor Ionescu, and Mubarak Shah. 2023. Diffusion Models in Vision: A Survey. *IEEE Transactions on Pattern Analysis and Machine Intelligence* 45, 9 (Sept. 2023), 10850–10869. [doi:10.1109/tpami.2023.3261988](https://doi.org/10.1109/tpami.2023.3261988)
- Chaorui Deng, Deyao Zhu, Kunchang Li, Chenhui Gou, Feng Li, Zeyu Wang, Shu Zhong, Weihao Yu, Xiaonan Nie, Ziang Song, Guang Shi, and Haoqi Fan. 2025. Emerging Properties in Unified Multimodal Pretraining. *arXiv preprint arXiv:2505.14683* (2025).
- Gen-3. 2024. Introducing Gen-3 Alpha: A New Frontier for Video Generation. <https://runwayml.com/research/introducing-gen-3-alpha/>.
- Michal Geyer, Omer Bar-Tal, Shai Bagon, and Tali Dekel. 2024. TokenFlow: Consistent Diffusion Features for Consistent Video Editing. In *ICLR*.

- Haoyang He, Jie Wang, Jiangning Zhang, Zhucun Xue, Xingyuan Bu, Qiangpeng Yang, Shilei Wen, and Lei Xie. 2025. OpenVE-3M: A Large-Scale High-Quality Dataset for Instruction-Guided Video Editing. *arXiv:2512.07826* (2025).
- Geoffrey Hinton, Oriol Vinyals, and Jeff Dean. 2015. Distilling the knowledge in a neural network. *arXiv preprint arXiv:1503.02531* (2015).
- Yi Huang, Jiancheng Huang, Yifan Liu, Mingfu Yan, Jiaxi Lv, Jianzhuang Liu, Wei Xiong, He Zhang, Lian-gliang Cao, and Shifeng Chen. 2025. Diffusion model-based image editing: A survey. *IEEE Transactions on Pattern Analysis and Machine Intelligence* (2025).
- Qing Jiang, Junan Huo, Xingyu Chen, Yuda Xiong, Zhaoyang Zeng, Yihao Chen, Tianhe Ren, Junzhi Yu, and Lei Zhang. 2025b. Detect Anything via Next Point Prediction. *arXiv:2510.12798* [cs.CV] <https://arxiv.org/abs/2510.12798>
- Zeyinzi Jiang, Zhen Han, Chaojie Mao, Jingfeng Zhang, Yulin Pan, and Yu Liu. 2025a. Vace: All-in-one video creation and editing. *arXiv:2503.07598* (2025).
- Alexander Kirillov, Eric Mintun, Nikhila Ravi, Hanzi Mao, Chloe Rolland, Laura Gustafson, Tete Xiao, Spencer Whitehead, Alexander C. Berg, Wan-Yen Lo, Piotr Dollar, and Ross Girshick. 2023. Segment Anything. In *ICCV*.
- Kling Team. 2024. KLING SPARK YOUR IMAGINATION. <https://kling.kuaishou.com/>.
- Weijie Kong, Qi Tian, Zijian Zhang, Rox Min, Zuozhuo Dai, Jin Zhou, Jiangfeng Xiong, Xin Li, Bo Wu, Jianwei Zhang, et al. 2024. Hunyuanyvideo: A systematic framework for large video generative models. *arXiv:2412.03603* (2024).
- Max Ku, Cong Wei, Weiming Ren, Huan Yang, and Wenhui Chen. 2024. AnyV2V: A plug-and-play framework for any video-to-video editing tasks. *TMLR* (2024).
- Black Forest Labs, Stephen Batifol, Andreas Blattmann, Frederic Boesel, Saksham Consul, Cyril Diagne, Tim Dockhorn, Jack English, Zion English, Patrick Esser, et al. 2025. FLUX. 1 Kontext: Flow Matching for In-Context Image Generation and Editing in Latent Space. *arXiv preprint arXiv:2506.15742* (2025).
- Zhen Li, Cheng-Ze Lu, Jianhua Qin, Chun-Le Guo, and Ming-Ming Cheng. 2022. Towards an end-to-end framework for flow-guided video inpainting. In *Proceedings of the IEEE/CVF conference on computer vision and pattern recognition*. 17562–17571.
- Xinyao Liao, Xianfang Zeng, Ziye Song, Zhoujie Fu, Gang Yu, and Guosheng Lin. 2025. In-Context Learning with Unpaired Clips for Instruction-based Video Editing. *arXiv:2510.14648* (2025).
- Yaron Lipman, Ricky TQ Chen, Heli Ben-Hamu, Maximilian Nickel, and Matt Le. 2022. Flow matching for generative modeling. *arXiv preprint arXiv:2210.02747* (2022).
- Yaron Lipman, Marton Havasi, Peter Holderith, Neta Shaul, Matt Le, Brian Karrer, Ricky TQ Chen, David Lopez-Paz, Heli Ben-Hamu, and Itai Gat. 2024. Flow matching guide and code. *arXiv preprint arXiv:2412.06264* (2024).
- Shaoteng Liu, Yuechen Zhang, Wenbo Li, Zhe Lin, and Jiaya Jia. 2024. Video-P2P: Video Editing with Cross-Attention Control. In *CVPR*.
- Xinyu Liu, Ailing Zeng, Wei Xue, Harry Yang, Wenhan Luo, Qifeng Liu, and Yike Guo. 2025. VFX Creator: Animated Visual Effect Generation with Controllable Diffusion Transformer. *arXiv preprint arXiv:2502.05979* (2025).
- Ilya Loshchilov and Frank Hutter. 2019. Decoupled Weight Decay Regularization. In *ICLR*.
- Guoqing Ma, Haoyang Huang, Kun Yan, Liangyu Chen, Nan Duan, Shengming Yin, Changyi Wan, Ranchen Ming, Xiaoniu Song, Xing Chen, et al. 2025. Step-video-t2v technical report: The practice, challenges, and future of video foundation model. *arXiv preprint arXiv:2502.10248* (2025).

- Andrew Melnik, Michal Ljubljjanac, Cong Lu, Qi Yan, Weiming Ren, and Helge Ritter. 2024. Video diffusion models: A survey. *arXiv preprint arXiv:2405.03150* (2024).
- Chong Mou, Mingdeng Cao, Xintao Wang, Zhaoyang Zhang, Ying Shan, and Jian Zhang. 2024. ReVideo: Remake a Video with Motion and Content Control. In *NeurIPS*.
- Chong Mou, Qichao Sun, Yanze Wu, Pengze Zhang, Xinghui Li, Fulong Ye, Songtao Zhao, and Qian He. 2025. InstructX: Towards Unified Visual Editing with MLLM Guidance. *arXiv:2510.08485*
- OpenAI. 2024. Sora: Creating video from text. <https://openai.com/index/sora/>.
- OpenAI. 2025. GPT-5 is here.
- Alibaba PAI. 2023. Wan2.1-Fun-14B-Control. <https://huggingface.co/alibaba-pai/Wan2.1-Fun-14B-Control>. Accessed: 2026-01-09.
- Federico Perazzi, Jordi Pont-Tuset, Brian McWilliams, Luc Van Gool, Markus Gross, and Alexander Sorkine-Hornung. 2016. A benchmark dataset and evaluation methodology for video object segmentation. In *Proceedings of the IEEE conference on computer vision and pattern recognition*. 724–732.
- Adam Polyak, Amit Zohar, Andrew Brown, Andros Tjandra, Animesh Sinha, Ann Lee, Apoorv Vyas, Bowen Shi, Chih-Yao Ma, Ching-Yao Chuang, et al. 2024. Movie gen: A cast of media foundation models. *arXiv:2410.13720* (2024).
- Colin Raffel, Noam Shazeer, Adam Roberts, Katherine Lee, Sharan Narang, Michael Matena, Yanqi Zhou, Wei Li, and Peter J Liu. 2020. Exploring the limits of transfer learning with a unified text-to-text transformer. *JMLR* (2020).
- Nikhila Ravi, Valentin Gabeur, Yuan-Ting Hu, Ronghang Hu, Chaitanya Ryali, Tengyu Ma, Haitham Khedr, Roman Rädle, Chloe Rolland, Laura Gustafson, et al. 2024. Sam 2: Segment anything in images and videos. *arXiv preprint arXiv:2408.00714* (2024).
- Nikhila Ravi, Valentin Gabeur, Yuan-Ting Hu, Ronghang Hu, Chaitanya Ryali, Tengyu Ma, Haitham Khedr, Roman Rädle, Chloe Rolland, Laura Gustafson, Eric Mintun, Junting Pan, Kalyan Vasudev Alwala, Nicolas Carion, Chao-Yuan Wu, Ross Girshick, Piotr Dollár, and Christoph Feichtenhofer. 2025. SAM 2: Segment Anything in Images and Videos. In *ICLR*.
- DecartAI Team. 2025a. Lucy Edit: Open-weight Text-guided Video Editing. Accessed: 2025-11-13.
- Gemma Team, Aishwarya Kamath, Johan Ferret, Shreya Pathak, Nino Vieillard, Ramona Merhej, Sarah Perrin, Tatiana Matejovicova, Alexandre Ramé, Morgane Rivière, et al. 2025b. Gemma 3 technical report. *arXiv preprint arXiv:2503.19786* (2025).
- Kling Team, Jialu Chen, Yuanzheng Ci, Xiangyu Du, Zipeng Feng, Kun Gai, Sainan Guo, Feng Han, Jingbin He, Kang He, et al. 2025a. Kling-Omni Technical Report. *arXiv preprint arXiv:2512.16776* (2025).
- Meituan LongCat Team, Hanghang Ma, Haoxian Tan, Jiale Huang, Junqiang Wu, Jun-Yan He, Lishuai Gao, Songlin Xiao, Xiaoming Wei, Xiaoqi Ma, et al. 2025c. Longcat-image technical report. *arXiv preprint arXiv:2512.07584* (2025).
- Qwen Team. 2025b. Qwen2.5-VL. <https://qwenlm.github.io/blog/qwen2.5-vl/>
- Alexandru Telea. 2004. An image inpainting technique based on the fast marching method. *Journal of graphics tools* (2004).
- Yuanpeng Tu, Hao Luo, Xi Chen, Sihui Ji, Xiang Bai, and Hengshuang Zhao. 2025. Videoanydoor: High-fidelity video object insertion with precise motion control. In *Proceedings of the Special Interest Group on Computer Graphics and Interactive Techniques Conference Conference Papers*. 1–11.

Team Wan, Ang Wang, Baole Ai, Bin Wen, Chaojie Mao, Chen-Wei Xie, Di Chen, Feiwu Yu, Haiming Zhao, Jianxiao Yang, Jianyuan Zeng, Jiayu Wang, Jingfeng Zhang, Jingren Zhou, Jinkai Wang, Jixuan Chen, Kai Zhu, Kang Zhao, Keyu Yan, Lianghua Huang, Mengyang Feng, Ningyi Zhang, Pandeng Li, Pingyu Wu, Ruihang Chu, Ruili Feng, Shiwei Zhang, Siyang Sun, Tao Fang, Tianxing Wang, Tianyi Gui, Tingyu Weng, Tong Shen, Wei Lin, Wei Wang, Wei Wang, Wenmeng Zhou, Wente Wang, Wenting Shen, Wenyuan Yu, Xianzhong Shi, Xiaoming Huang, Xin Xu, Yan Kou, Yangyu Lv, Yifei Li, Yijing Liu, Yiming Wang, Yingya Zhang, Yitong Huang, Yong Li, You Wu, Yu Liu, Yulin Pan, Yun Zheng, Yuntao Hong, Yupeng Shi, Yutong Feng, Zeyinzi Jiang, Zhen Han, Zhi-Fan Wu, and Ziyu Liu. 2025. Wan: Open and Advanced Large-Scale Video Generative Models. *arXiv preprint arXiv:2503.20314* (2025).

Guo-Hua Wang, Shanshan Zhao, Xinjie Zhang, Liangfu Cao, Pengxin Zhan, Lunhao Duan, Shiyin Lu, Minghao Fu, Xiaohao Chen, Jianshan Zhao, et al. 2025. Ovis-U1 Technical Report. *arXiv preprint arXiv:2506.23044* (2025).

Zhou Wang, Alan C Bovik, Hamid R Sheikh, and Eero P Simoncelli. 2004. Image quality assessment: from error visibility to structural similarity. *IEEE Transactions on Image Processing* 13, 4 (2004), 600–612.

Cong Wei, Quande Liu, Zixuan Ye, QiuLin Wang, Xintao Wang, Pengfei Wan, Kun Gai, and Wenhui Chen. 2025. Univideo: Unified understanding, generation, and editing for videos. *arXiv preprint arXiv:2510.08377* (2025).

Thaddäus Wiedemer, Yuxuan Li, Paul Vicol, Shixiang Shane Gu, Nick Matarese, Kevin Swersky, Been Kim, Priyank Jaini, and Robert Geirhos. 2025. Video models are zero-shot learners and reasoners. *arXiv preprint arXiv:2509.20328* (2025).

Wikipedia contributors. 2024. Peak signal-to-noise ratio — Wikipedia, The Free Encyclopedia. https://en.wikipedia.org/w/index.php?title=Peak_signal-to-noise_ratio&oldid=1210897995 [Online; accessed 4-March-2024].

Chenfei Wu, Jiahao Li, Jingren Zhou, Junyang Lin, Kaiyuan Gao, Kun Yan, Shengming Yin, Shuai Bai, Xiao Xu, Yilei Chen, Yuxiang Chen, Zecheng Tang, Zekai Zhang, Zhengyi Wang, An Yang, Bowen Yu, Chen Cheng, Dayiheng Liu, Deqing Li, Hang Zhang, Hao Meng, Hu Wei, Jingyuan Ni, Kai Chen, Kuan Cao, Liang Peng, Lin Qu, Minggang Wu, Peng Wang, Shuting Yu, Tingkun Wen, Wensen Feng, Xiaoxiao Xu, Yi Wang, Yichang Zhang, Yongqiang Zhu, Yujia Wu, Yuxuan Cai, and Zenan Liu. 2025b. Qwen-Image Technical Report. arXiv:2508.02324 [cs.CV] <https://arxiv.org/abs/2508.02324>

Jay Zhangjie Wu, Yixiao Ge, Xintao Wang, Stan Weixian Lei, Yuchao Gu, Yufei Shi, Wynne Hsu, Ying Shan, Xiaohu Qie, and Mike Zheng Shou. 2023. Tune-A-Video: One-Shot Tuning of Image Diffusion Models for Text-to-Video Generation. In *ICCV*.

Yuhui Wu, Liyi Chen, Ruibin Li, Shihao Wang, Chenxi Xie, and Lei Zhang. 2025a. InsViE-1M: Effective Instruction-based Video Editing with Elaborate Dataset Construction. In *ICCV*.

Zhihan Xiao, Lin Liu, Yixin Gao, Xiaopeng Zhang, Haoxuan Che, Songping Mai, and Qi Tian. 2025. LoVoRA: Text-guided and Mask-free Video Object Removal and Addition with Learnable Object-aware Localization. arXiv:2512.02933

Ming Xie, Junqiu Yu, Qiaole Dong, Xiangyang Xue, and Yanwei Fu. 2025. Enhancing Video Inpainting with Aligned Frame Interval Guidance. arXiv:2510.21461 [cs.CV] <https://arxiv.org/abs/2510.21461>

Zhen Xing, Qijun Feng, Haoran Chen, Qi Dai, Han Hu, Hang Xu, Zuxuan Wu, and Yu-Gang Jiang. 2024. A survey on video diffusion models. *Comput. Surveys* 57, 2 (2024), 1–42.

Shiyuan Yang, Zheng Gu, Liang Hou, Xin Tao, Pengfei Wan, Xiaodong Chen, and Jing Liao. 2025a. MTV-Inpaint: Multi-Task Long Video Inpainting. *arXiv:2503.11412* (2025).

Xiangpeng Yang, Ji Xie, Yiyuan Yang, Yan Huang, Min Xu, and Qiang Wu. 2025c. Unified Video Editing with Temporal Reasoner. *arXiv preprint arXiv:2512.07469* (2025).

Zhuoyi Yang, Jiayan Teng, Wendi Zheng, Ming Ding, Shiyu Huang, Jiazheng Xu, Yuanming Yang, Wenyi Hong, Xiaohan Zhang, Guanyu Feng, Da Yin, Xiaotao Gu, Yuxuan Zhang, Weihan Wang, Yean Cheng, Ting Liu, Bin Xu, Yuxiao Dong, and Jie Tang. 2025b. CogVideoX: Text-to-Video Diffusion Models with An Expert Transformer. In *ICLR*.

Zixuan Ye, Xuanhua He, Quande Liu, Qiulin Wang, Xintao Wang, Pengfei Wan, Di Zhang, Kun Gai, Qifeng Chen, and Wenhan Luo. 2025. UNIC: Unified In-Context Video Editing. arXiv:2506.04216

Richard Zhang, Phillip Isola, Alexei A Efros, Eli Shechtman, and Oliver Wang. 2018. The unreasonable effectiveness of deep features as a perceptual metric. In *CVPR*. 586–595.

Zhongwei Zhang, Fuchen Long, Wei Li, Zhaofan Qiu, Wu Liu, Ting Yao, and Tao Mei. 2025. Region-Constraint In-Context Generation for Instructional Video Editing. *arXiv:2512.17650* (2025).

Zhixing Zhang, Bichen Wu, Xiaoyan Wang, Yaqiao Luo, Luxin Zhang, Yinan Zhao, Peter Vajda, Dimitris Metaxas, and Licheng Yu. 2023. AVID: Any-Length Video Inpainting with Diffusion Model. *arXiv:2312.03816* (2023).

Bojia Zi, Weixuan Peng, Xianbiao Qi, Jianan Wang, Shihao Zhao, Rong Xiao, and Kam-Fai Wong. 2025a. MiniMax-Remover: Taming Bad Noise Helps Video Object Removal. In *NeurIPS*.

Bojia Zi, Penghui Ruan, Marco Chen, Xianbiao Qi, Shaozhe Hao, Shihao Zhao, Youze Huang, Bin Liang, Rong Xiao, and Kam-Fai Wong. 2025b. Senorita-2M: A High-Quality Instruction-based Dataset for General Video Editing by Video Specialists. In *NeurIPS Dataset and Benchmark Track*.

Bojia Zi, Shihao Zhao, Xianbiao Qi, Jianan Wang, Yukai Shi, Qianyu Chen, Bin Liang, Kam-Fai Wong, and Lei Zhang. 2025c. CoCoCo: Improving Text-Guided Video Inpainting for Better Consistency, Controllability and Compatibility. In *AAAI*.

A User study

To evaluate the perceptual alignment of our method with human judgment, we conduct a formal user study comparing our approach against four state-of-the-art baselines: two instruction-based and two mask-based methods. We recruit 21 participants to assess the editing results. For each test case, users are presented with the original and edited videos and are asked to rate the performance on a 5-point Likert scale across three dimensions:

- Generative Quality: This metric assesses the realism of the inserted objects, their alignment with the text prompts (in terms of appearance and motion), and the presence of temporal artifacts such as flickering or jitter.
- Background Preservation: We evaluate the model’s ability to maintain the integrity of the original scene, ensuring that non-target regions remain unmodified and the overall visual style stays consistent.
- Spatial Accuracy: This criterion focuses on the plausibility of the spatial layout, including the accuracy of object positioning, scale proportions, and the correctness of occlusion relationships with the environment.

Table 6 User study. We conduct a user study comparing our method with two mask-based and two instruction-based state-of-the-art video editing models. Red and blue indicate the best and second-best performance.

Method	Generative Quality	Background Preservation	Spatial Accuracy	Overall
Lucy	2.152	2.852	2.204	2.403
UniVideo	2.652	2.809	2.357	2.606
Video Painter	2.619	2.953	2.847	2.807
Vace	2.000	2.952	2.333	2.429
Ours	3.858	4.181	4.157	4.065

B Failure Case



Figure 7 Failure Case. When the scene involves high-speed motion or only the initial frame is annotated, the inserted object may suddenly disappear.

While our model can insert static or dynamic objects into both static and moving scenes, failures may still occur in videos characterized by large-scale motion or significant camera shake. Additionally, insufficiently

dense annotations can lead to insertion failures. For instance, if a point is provided only in one frame, the inserted object might disappear in subsequent frames. Addressing these limitations is reserved for future work. Visual examples of these failure cases are shown in Fig. 7.

C Ablation Study on Sparse Point and Dense Mask Input

The difficulty of the object insertion task varies significantly depending on the type of control input provided. To investigate this, we trained two separate models, one guided exclusively by **sparse points** and the other by **dense mask**, and evaluated their performance after an equal number of training iterations.

As illustrated in Figure 2b, precise frame-by-frame mask guidance provides the model with explicit localization and boundary information, thereby significantly lowering the barrier for successful object insertion. In contrast, achieving precise insertion under sparse point conditions presents a much greater challenge. In the absence of additional boundary information, the model must independently determine the editing contours. After same training steps, the model struggles to establish a robust mapping between semantic concepts and the generation of object silhouettes. This often leads to distorted outlines, incomplete or misaligned boundaries, or failed generations resulting in blurred color patches.

The quantitative metrics presented in Tab. 7 further substantiate the increased complexity of the point-guided task. In this setting, the model is required to synthesize the insertion position, the temporal video context, and the textual conditions simultaneously. The results indicate that the mask-based model outperforms the point-based model by 4.99 in PSNR and 1.65 in LPIPS, respectively, thanks to the clear object boundaries provided by the masks. The mask-guided approach consistently demonstrates superior performance across other metrics as well, further highlighting the inherent advantages of dense signals over sparse signals for fine-grained control. This observation inspired our development of a two-stage training strategy and a mask-to-point distillation method, which facilitates an effective transition from dense to sparse control signals.

Table 7 Ablation Studies on Control Signal Settings. We conduct experiments using points and masks as control during both training and inference. To ensure a fair comparison, all other experimental settings—including the dataset, architecture, and training iterations—are held constant. The results demonstrate that the mask-based method consistently outperforms the point-based counterpart in background preservation, semantic alignment, and temporal consistency. This performance gain is attributed to the explicit spatiotemporal boundaries and denser control inherent in masks.

	MSE ↓	MAE ↓	PSNR ↑	SSIM ↑	LPIPS _{×100} ↓	CLIP BG ↑	CLIP TA ↑	CLIP TC ↑	EWarp ↓
Mask	65.58	2.30	36.66	0.9714	1.79	24.28	23.38	99.34	0.35
Point	133.41	5.23	31.67	0.9433	3.44	24.35	23.02	99.25	0.38

D Model Parameter

In this section, we briefly describe the architectures and parameter sizes of different baselines. As summarized in Tab. 1, we group existing methods into two categories: **instruction-based** video editing methods and **mask-based** video editing methods. The reported *Model Size* corresponds to the parameters required at inference time. When a method relies on additional models (e.g., for multimodal understanding or inpainting/filling), we report the total size in the form of “A+B”.

Instruction-based methods.

- **Ditto** [Bai et al. \(2025\)](#) is built upon Wan 2.1-T2V-14B [Wan et al. \(2025\)](#) and trains an additional 0.2B LoRA for editing adaptation.
- **Lucy Team** [\(2025a\)](#) is based on Wan 2.2-T2V-5B, resulting in a 5B-scale instruction-driven editing model.

- **ICVE** [Liao et al. \(2025\)](#) is built upon HunyuanVideo-T2V-13B [Kong et al. \(2024\)](#), forming a 13B instruction-based video editing model.
- **UniVideo** [Wei et al. \(2025\)](#) adopts a HunyuanVideo backbone and integrates Qwen-VL-2.5-7B [Team \(2025b\)](#) for multimodal understanding, resulting in a total size of 13B+7B.
- **VideoCoF** [Yang et al. \(2025c\)](#) is based on Wan-2.1-T2V-14B with a model size of 14B.

Mask-based methods.

- **Senorita** [Zi et al. \(2025b\)](#) uses CogVideoX-5B-I2V [Yang et al. \(2025b\)](#) as the backbone and employs FLUX.1-Fill [dev] 12B [Black Forest Labs \(2024\)](#) for first-frame guided filling/editing, resulting in a total of 5B+12B.
- **VideoPainter** [Bian et al. \(2025\)](#) adopts the same backbone and filling model as Senorita, hence also 5B+12B.
- **Vace** [Jiang et al. \(2025a\)](#) adopts a context-adaptation architecture, built on Wan 2.1-T2V-1.3B with an additional 0.3B adaptation module, yielding 1.3B+0.3B in total.

Our method requires only a 1.3B parameter model at inference time while achieving SOTA editing performance.

E MLLM Evaluation Accuracy

To rigorously assess the video editing performance, we employ state-of-the-art Multimodal Large Language Models (MLLMs), specifically Gemini3-Pro [Team et al. \(2025b\)](#) and GPT-5.2 [OpenAI \(2025\)](#), as automated evaluators. To validate the reliability of these model-based metrics, we conduct a comparative analysis against human-annotated ground truth.

For the **Gemini3-Pro** evaluation, we randomly sampled 600 instances for human-model alignment verification. Each test case consists of an original-edited image pair, where a red bounding box defines the target Region of Interest (ROI). The models are tasked with identifying whether the requested object was successfully synthesized within the designated ROI. Gemini3-Pro achieves a high agreement rate of 97.2% with human annotators. Qualitative analysis of the remaining 2.8% discrepancies reveals that most errors stem from inherent semantic ambiguities at transitional boundaries—for instance, distinguishing forest elements from adjacent grassland. In such boundary regions, pre-existing visual contexts often confound the model’s categorical judgment.

Gemini Prompt

You will see two images and an editing instruction: the first is the original image, and the second is the target image.

Analyze the provided information and answer the following questions:

1. **Object Addition Detection:** Was a new object added inside the red bounding box?
2. **Semantic Alignment Scoring:** Evaluate the semantic consistency between the object in the red box and the given prompt, Give a score from 1 to 5.
3. **Visual Quality Scoring:** Evaluate the visual quality of the added object, considering edge blending, lighting and shadow consistency, texture realism, perspective alignment, and overall coherence with the background. Give a score from 1 to 5.

Return your response strictly in the following JSON format:

```
{
  "has_added_object_in_red_box": true/false,
```

```

    "text_alignment": {
        "score": 1-5,
        "comments": "Brief explanation of the semantic assessment"
    },
    "visual_quality": {
        "score": 1-5,
        "comments": "Brief explanation of the quality assessment"
    },
    "reasoning": "Concise justification for all answers above"
}

```

Do not include any additional text outside the JSON block.

We further evaluate **GPT-5.2** assessment accuracy using 200 randomly selected samples under the same task formulation. GPT-5.2 demonstrates a 96% alignment with human judgment. A granular error analysis of the eight discrepant cases identifies one false negative and seven false positives. We observe that false positives primarily occur when the synthesized object is localized near but strictly outside the bounding box, suggesting a slight misalignment in the model's spatial reasoning relative to the explicit ROI constraints.

GPT Prompt

You will see two images and an editing instruction: the first is the original image, and the second is the target image.

Analyze the provided information and answer the following questions:

- Object Addition Detection:** Was a new object added inside the red bounding box?
- Semantic Alignment Scoring:** Evaluate the semantic consistency between the object in the red box and the given prompt. Score from 1 (completely inconsistent) to 5 (matches the prompt).
- Visual Quality Scoring:** Evaluate the visual quality of the added object (if any), considering factors such as edge blending, lighting/shadow consistency, texture realism, perspective alignment, and overall coherence with the background. Provide a quality score from 1 to 5 (5 = photorealistic and seamless; 1 = obvious artifact or poor integration).

Return your response strictly in the following JSON format:

```

{
    "has_added_object_in_red_box": true/false,
    "text_alignment": {
        "score": 1-5,
        "comments": "Brief explanation of the semantic assessment"
    },
    "visual_quality": {
        "score": 1-5,
        "comments": "Brief explanation of the quality assessment"
    },
    "reasoning": "Concise justification for all answers above"
}

```

Do not include any additional text outside the JSON block.



Figure 8 Mask-based Video Editing results. Using video and mask frames inputs, we compare the qualitative performance of VACE, VideoPainter, and our proposed method. While VACE occasionally fails to generate the target object and VideoPainter exhibits noticeable artifacts around object boundaries, our method consistently produces high-quality, semantically aligned editing results.